Optimized Design of an Instrumented Spatial Linkage that Minimizes Errors in Locating the Rotational Axes of the Tibiofemoral Joint: A Computational Analysis

Daniel P. Bonny
Biomedical Engineering Graduate Group,
University of California, Davis,
One Shields Ave,
Davis, CA 95616-5270

M. L. Hull[1]
Department of Mechanical Engineering,
Department of Biomedical Engineering,
University of California, Davis,
One Shields Ave,
Davis, CA 95616-5270
e-mail: mlhull@ucdavis.edu

S. M. Howell
Biomedical Engineering Graduate Group,
Department of Mechanical Engineering,
University of California, Davis,
One Shields Ave,
Davis, CA 95616-5270

*An accurate method to locate of the flexion-extension (F-E) axis and longitudinal rotation (LR) axis of the tibiofemoral joint is required to accurately characterize tibiofemoral kinematics. A method was recently developed to locate these axes using an instrumented spatial linkage (ISL) (2012, "On the Estimate of the Two Dominant Axes of the Knee Using an Instrumented Spatial Linkage," J. Appl. Biomech., **28**(2), pp. 200–209). However, a more comprehensive error analysis is needed to optimize the design and characterize the limitations of the device before using it experimentally. To better understand the errors in the use of an ISL in finding the F-E and LR axes, our objectives were to (1) develop a method to computationally determine the orientation and position errors in locating the F-E and LR axes due to transducer nonlinearity and hysteresis, ISL size and attachment position, and the pattern of applied tibiofemoral motion, (2) determine the optimal size and attachment position of an ISL to minimize these errors, (3) determine the best pattern of pattern of applied motion to minimize these errors, and (4) examine the sensitivity of the errors to range of flexion and internal-external (I-E) rotation. A mathematical model was created that consisted of a virtual "elbow-type" ISL that measured motion across a virtual tibiofemoral joint. Two orientation and two position errors were computed for each axis by simulating the axis-finding method for 200 iterations while adding transducer errors to the revolute joints of the virtual ISL. The ISL size and position that minimized these errors were determined from 1080 different combinations. The errors in locating the axes using the optimal ISL were calculated for each of three patterns of motion applied to the tibiofemoral joint, consisting of a sequential pattern of discrete tibiofemoral positions, a random pattern of discrete tibiofemoral positions, and a sequential pattern of continuous tibiofemoral positions. Finally, errors as a function of range of flexion and I-E rotation were determined using the optimal pattern of applied motion. An ISL that was attached to the anterior aspect of the knee with 300-mm link lengths had the lowest maximum error without colliding with the anatomy of the joint. A sequential pattern of discrete tibiofemoral positions limited the largest orientation or position error without displaying large bias error. Finally, the minimum range of applied motion that ensured all errors were below 1 deg or 1 mm was 30 deg flexion with ± 15 deg I-E rotation. Thus a method for comprehensive analysis of error when using this axis-finding method has been established, and was used to determine the optimal ISL and range of applied motion; this method of analysis could be used to determine the errors for any ISL size and position, any applied motion, and potentially any anatomical joint.*
[DOI: 10.1115/1.4023135]

1 Introduction

Characterizing kinematics of the tibiofemoral joint requires accurately locating the axes of motion. It is generally accepted that rotation of the tibiofemoral joint involves motions about two axes: the flexion-extension (F-E) axis and longitudinal rotation (LR) axis [1]. The primary axis, the F-E axis about which flexion-extension of the tibia relative to the femur occurs, is fixed in the femur and is approximately parallel to the posterior and distal femoral condyles [1,2]. The secondary axis, the LR axis about which internal-external (I-E) rotation of the tibia relative the femur occurs, is fixed in the tibia approximately perpendicular to the F-E axis [1,3]. At any flexion angle and without external loads applied to the tibiofemoral joint, the relative positions of the femur and tibia are fully described by these two kinematic axes [1,3]. Incorrectly locating these axes can result in inaccurate measures of flexion angle and amount of rotation [4] and introduce erroneous coupled motions during measurement of

[1]Corresponding author.
Contributed by the Bioengineering Division of ASME for publication in the Journal of Biomechanical Engineering. Manuscript received May 7, 2012; final manuscript received October 22, 2012; accepted manuscript posted December 8, 2012; published online February 11, 2013. Assoc. Editor: Sean S. Kohles.

screw-home motion and during gait analysis [5,6]. Approximations of the F-E axis are commonly used to determine prosthesis placement in total knee arthroplasty (TKA) [7–10]; incorrectly locating the F-E axis can result in incorrect placement of the prostheses [2,11]. In addition, the design of the TKA prostheses can affect the location of the kinematic axes and thus affect tibiofemoral kinematics [12]. Therefore when locating the F-E and LR axes, an accurate and precise axis-finding method is required.

Several previous methods have been developed for determining the F-E and LR axes, but each has limitations. A mechanical axis finder used by Hollister et al. [1] determined the axis of rotation of a hinge joint using subjective visual alignment which resulted in relatively high orientation and position errors of 1.5 deg and 1 mm. The compound hinge method, a mathematical calculation of two fixed axes of rotation, was described by Churchill et al. [7]; however, accuracy was not defined, and the mathematical description is too vague to reproduce the method. More recently, Roland et al. [13,14] developed the Virtual Axis Finder using mathematical optimization in conjunction with either video-based motion analysis or roentgen stereophotogrammetric analysis (RSA). Using video-based motion analysis, this method achieved root mean squared errors (RMSE) of 0.26 deg and 0.28 mm when locating the LR axis and 0.36 deg and 0.25 mm when locating the F-E axis. However, the motion analysis equipment requires constant line-of-sight and is expensive, and the less-accurate RSA requires a radiolucent test fixture.

An alternative to the methods above is the instrumented spatial linkage (ISL), which offers the potential to provide a low-cost, accurate means to locate the F-E and LR axes. The ISL has been used broadly to measure motion of the tibiofemoral joint [15–34], achieving orientation and position RMSEs as low as 0.83 deg and 0.73 mm [34]. Other studies have used an ISL to locate the screw axis of an anatomical joint [15,17,18,35]. Only one study known to the authors has demonstrated an ISL to locate the F-E and LR axes [36]. Gatti [36] developed a new mathematical framework to simultaneously locate the F-E and LR axes with an ISL, thus eliminating the need to independently locate these axes [1,13,14].

Although the mathematical framework of Gatti's [36] axis-finding method using an ISL was thoroughly described, the analysis of errors was limited. In the original validation of this method, the orientation and position errors in locating the F-E and LR axes were statistically determined using a simulated ISL and varying the size of a virtual tibiofemoral joint [36]. However, only encoder resolution error was examined [36]; additional error sources include nonlinearity and hysteresis of the ISL revolute joint transducers and signal noise. Also, only one combination of ISL size and attachment position was examined, hence limiting the interpretation of the errors to a particular ISL [36]. Simulating a range of variables that describe the size and attachment position of the ISL would determine the best ISL configuration to locate the F-E and LR axes with minimal errors. Finally, only one pattern of applied motion was examined [36]. Varying the order (i.e. sequential versus random), resolution, and the range of applied motion would determine the effectiveness of the axis-finding method under more general conditions.

The first objective was to develop a method to computationally determine the bias, precision, and RMSE in locating the F-E and LR axes due to sources of transducer error for a given ISL configuration and pattern of applied motion as well as present this data in the context of anatomically relevant coordinate systems. The second objective was to define the ISL size and attachment position that locates the F-E and LR axes with minimal errors using this method. The third objective was to use the ISL defined in Objective 2 to define the pattern of applied motion to locate the F-E and LR axes with minimal errors. The final objective was to determine the sensitivity of the bias errors, precision errors, and RMSEs to the ranges of applied flexion and I-E rotation.

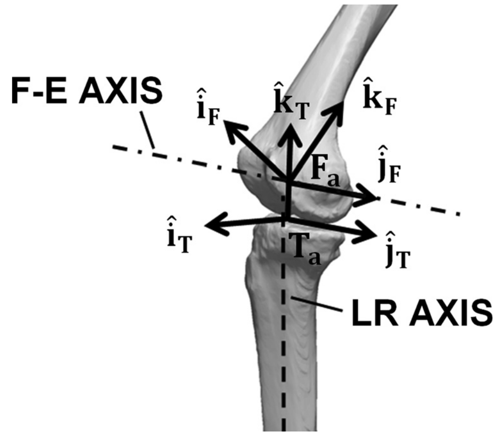

Fig. 1 The virtual tibiofemoral joint. The F-E axis was perpendicular to the $\hat{i}_F\hat{k}_F$-plane and passed through the origin of the femoral anatomic coordinate system. The LR axis was perpendicular to the $\hat{i}_T\hat{j}_T$-plane and passed 2.5 mm anterior to the origin tibial anatomic coordinate system.

2 Methods

2.1 The Virtual Tibiofemoral Joint. A virtual tibiofemoral joint consisting of two nonintersecting, perpendicular axes [1] was created to simulate tibiofemoral kinematics. This virtual tibiofemoral joint was described by two coordinate systems: the femoral anatomic coordinate system and the tibial anatomic coordinate system (Fig. 1). The tibial anatomic coordinate system was the global coordinate system, and the origin was denoted by T_a. The axes of the tibial anatomic coordinate system were defined such that $\hat{\mathbf{i}}_\mathbf{T}$ was oriented anteriorly, $\hat{\mathbf{k}}_\mathbf{T}$ was oriented proximally, and $\hat{\mathbf{j}}_\mathbf{T}$ was defined as the cross-product of the $\hat{\mathbf{k}}_\mathbf{T}$ and $\hat{\mathbf{i}}_\mathbf{T}$ axes. The femoral anatomic coordinate system origin, denoted by F_a, was defined at full extension to lie on the $\hat{\mathbf{k}}_\mathbf{T}$ axis and 20 mm proximal to the origin T_a; 20 mm is the approximate radius of the femoral condyles (r_{cond}) [37]. The axes of the femoral anatomic coordinate system had the same orientation at full extension as the axes of the tibial anatomic coordinate system. A standard F-E axis was established perpendicular to the sagittal ($\hat{\mathbf{i}}_\mathbf{F}\hat{\mathbf{k}}_\mathbf{F}$) plane, passing through the origin F_a. A standard LR axis was established perpendicular to the transverse ($\hat{\mathbf{i}}_\mathbf{T}\hat{\mathbf{j}}_\mathbf{T}$) plane, passing 2.5 mm anterior to the origin T_a [1].

Two orientations and two positions were used to describe each of the tibiofemoral axes with reference to the anatomic coordinate systems. The two orientations of the F-E axis, I-E and varus-valgus (V-V) rotations, were defined as the projection angles of the axis on the $\hat{\mathbf{i}}_\mathbf{F}\hat{\mathbf{j}}_\mathbf{F}$-plane and $\hat{\mathbf{j}}_\mathbf{F}\hat{\mathbf{k}}_\mathbf{F}$-plane respectively. The two orientations of the LR axis, V-V and F-E rotations, were defined as the projection angles of the axis on the $\hat{\mathbf{j}}_\mathbf{T}\hat{\mathbf{k}}_\mathbf{T}$-plane and the $\hat{\mathbf{i}}_\mathbf{T}\hat{\mathbf{k}}_\mathbf{T}$-plane respectively. The two positions of the F-E axis, the anterior-posterior (A-P) and proximal-distal (P-D) positions, were defined as the coordinates where the F-E axis intersects the $\hat{\mathbf{i}}_\mathbf{F}\hat{\mathbf{k}}_\mathbf{F}$-plane in the $\hat{\mathbf{i}}_\mathbf{F}$ and $\hat{\mathbf{k}}_\mathbf{F}$ directions, respectively. The two positions of the LR axis, the A-P and medial-lateral (M-L) positions, were defined as the coordinates where the LR axis intersects the $\hat{\mathbf{i}}_\mathbf{T}\hat{\mathbf{j}}_\mathbf{T}$-plane in the $\hat{\mathbf{i}}_\mathbf{T}$ and $\hat{\mathbf{j}}_\mathbf{T}$ directions, respectively. Thus, eight dependent variables describe the location of the F-E and LR axes. Of the eight parameters describing the positions and orientations of the standard F-E and LR axes relative to the femoral anatomic and tibial anatomic coordinate systems respectively, only the A-P position of the LR axis was nonzero.

Simulated tibiofemoral motion was applied via a transformation matrix from the tibial anatomic coordinate system to the femoral anatomic coordinate system, defined as $\left[\mathbf{T}_{\mathbf{Fa/Ta}}\right]_1$; this transformation matrix was computed using consecutive transformation matrix multiplication [38]. Each transformation matrix was either a simple rotation transformation matrix $\mathrm{Rot}(\mathbf{a},b)$ or a simple

Table 1 The Denavit-Hartenberg parameters describing the virtual ISL (α_k, a_k, s_k, and the revolute joint offset θ_k) for each link k were a function of the "elbow" angle φ at full extension, the link length l, and whether the ISL "wrist" was attached to the femur or tibia

	"Wrist" on Tibia				"Wrist" on Femur			
Link k	α_k (deg)	a_k (mm)	s_k (mm)	θ_k offset (deg)	α_k (deg)	a_k (mm)	s_k (mm)	θ_k offset (deg)
1	0	0	0	$180-\phi/2$	90	0	0	$90-\phi/2$
2	90	0	0	270	90	0	l	0
3	90	0	0	90	90	l	0	$-\phi-90$
4	90	l	0	$-\phi-90$	90	0	0	90
5	90	0	l	0	90	0	0	270
6	90	0	0	$180-\phi/2$	0	0	0	$180-\phi/2$

translation transformation matrix Trans(**a**,b), where **a** was either the axis of rotation or translation respectively and where b was either the amount of rotation or translation respectively. With the tibial anatomic coordinate system as the fixed (or "base") coordinate system, the first transformation matrix $\mathrm{Trans}(z, r_{\mathrm{cond}})$ represented the first step in establishing the femoral coordinate system; this transformation matrix defined the position of the origin of the femoral coordinate system to be $r_{\mathrm{cond}} = 20$ mm proximal to the tibial coordinate system. I-E rotation about the LR axis was simulated via a simple rotation transformation matrix about the $\hat{\mathbf{k}}_{\mathbf{T}}$-axis, $\mathrm{Rot}(z, \theta_{I-E})$; this rotation matrix was pre- and post-multiplied by the simple translation transformation matrixes $\mathrm{Trans}(x, 2.5\mathrm{mm})$ and $\mathrm{Trans}(x,\ -2.5\ \mathrm{mm})$ respectively to represent the 2.5 mm offset of the LR axis from the tibial anatomic coordinate system. Finally, flexion-extension was simulated via a simple rotation transformation matrix about the $\hat{\mathbf{j}}_{\mathbf{F}}$-axis, $\mathrm{Rot}(y, -\theta_F)$; flexion corresponded to a negative rotation about this axis. Thus the overall transformation matrix between the tibial anatomic coordinate system and the femoral coordinate system at any flexion angle θ_F and I-E rotation angle θ_{I-E} was:

$$\left[\mathbf{T}_{\mathbf{Fa/Ta}}\right]_1 = \mathrm{Trans}(z, r_{\mathrm{cond}}) \cdot \mathrm{Trans}(x, 2.5\ \mathrm{mm}) \cdot \mathrm{Rot}(z, \theta_{I-E}) \cdot \mathrm{Trans}(x, -2.5\ \mathrm{mm}) \cdot \mathrm{Rot}(y, -\theta_F) \tag{1}$$

The pattern of applied motion consisted of a set of flexion and I-E rotation angles defined by several independent variables. Two independent variables were the maximum flexion angle measured from full extension and the maximum range of I-E rotation. The remaining independent variables depended on the category of motion, either "random discrete," "sequential discrete," or "sequential continuous." In "random discrete" motion, each set of flexion and I-E rotation angles was determined randomly with the number of sampling locations as the independent variable. In "sequential discrete" and "sequential continuous" motions, each set of flexion and I-E rotation angles was predetermined. Both "sequential" motions were characterized by I-E rotation cycles throughout flexion; each cycle consisted of I-E rotation from 0 deg to the internal rotation limit, followed by rotation from the minimum angle to the external rotation limit, followed by rotation back to 0 deg. In "sequential discrete" motion, these I-E rotation cycles were applied with flexion held constant at discrete angles. In "sequential continuous" motion, these I-E rotation cycles were applied during continuously applied flexion. The number of I-E rotation cycles was an independent variable for both "sequential discrete" and "sequential continuous" motions. The final independent variable for "sequential discrete" and "sequential continuous" motions was the I-E rotation resolution (i.e. the I-E rotation angle between each simulated tibiofemoral position), which was 5 deg for "sequential discrete" motion and 0.5 deg for "sequential continuous" motion.

2.2 The Virtual ISL. A virtual ISL was created to measure motions across the virtual tibiofemoral joint. The ISL was described by Denavit–Hartenberg parameter notation [39], and was a standard "elbow-type" linkage, which had a "wrist" consisting three intersecting revolute joints axes, an "elbow" consisting of one revolute joint, and a "shoulder" consisting of two intersecting revolute joint axes [40]. An "elbow-type" linkage was chosen because this type of linkage both maximizes the reachable volume of a linkage (i.e., workspace) relative to the size of the linkage, and is able to reach all orientations and positions in that workspace [40]. For an "elbow-type" ISL, all Denavit–Hartenberg twist angles were either 0 deg or 90 deg, and for each link either the length was zero, the joint offset was zero, or both were zero [40]. The revolute joint axis of each link was $\hat{\mathbf{k}}$. The transformation matrix from the coordinate system of link 1 to the coordinate system of link 7 was defined as $[\mathbf{T}]_{\mathbf{ISL}}$.

Three independent variables were created to describe the Denavit–Hartenberg parameters (i.e., the size) of the ISL (Table 1). The first independent variable was categorical and defined whether the ISL "wrist" was attached to the tibia or the femur; the Denavit–Hartenberg parameters were different depending on whether the "wrist" was attached to the tibia or the femur (Fig. 2, Table 1). The second independent variable, l, was defined as either the length of link 3 and the joint offset of link 4 if the "wrist" was attached to the tibia, or the length of link 2 and the joint offset of link 3 if the "wrist" was attached to the femur. The third independent variable, ϕ, was defined as the angle of the ISL "elbow" at full extension of the tibiofemoral joint; this angle was also used to determine the distance between the ISL "wrist" and "shoulder" at full extension, defined as d_{ws}. Thus two of the Denavit–Hartenberg parameters were defined by the independent variable l, six of the revolute joint offsets were defined by the independent variables ϕ and the categorical variable defining whether the "wrist" was attached to the femur or tibia, and the remaining twist angles and link lengths were fixed.

Three independent variables were created to describe the attachment position of the ISL on the virtual tibiofemoral joint by

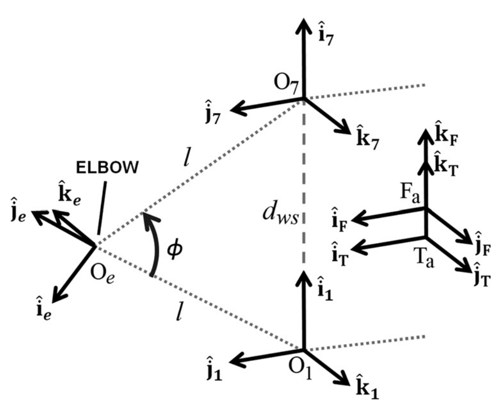

Fig. 2 The variables describing the size of the virtual ISL, shown with the coordinate systems of the virtual tibiofemoral joint at full extension, were the link length l and the "elbow" angle ϕ. If the ISL "wrist" was attached to tibia, the "elbow" was the origin of link 4 ($e = 4$). If the ISL "wrist" was attached to femur, the "elbow" was the origin of link 3 ($e = 3$).

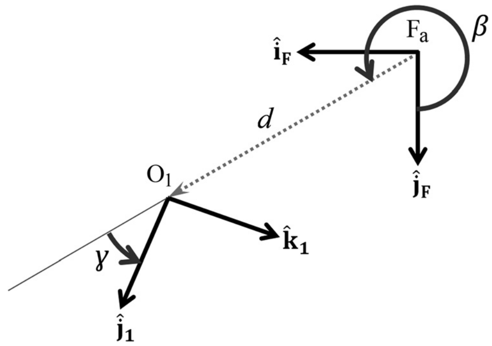

Fig. 3 The variables describing attachment position of the virtual ISL, shown with the femoral anatomic coordinate system of the virtual tibiofemoral joint, transverse view. The variable β defined the angular position of the ISL attachment about the tibiofemoral joint, the variable d defined the distance of the ISL "wrist" and "shoulder" from the $\hat{\mathbf{k}}_\mathbf{F}$ axis, and the variable γ defined the orientation of the axes of the revolute joints of ISL links 1 and 6 at full extension.

defining the positions and orientations of the coordinate systems of the first and last ISL links. The ISL was defined at full extension such that the origins of links 1 and 7 (O_1 and O_7) were a distance of $0.5 \cdot d_{ws}$ from the origin $\mathrm{F_a}$ in the $-\hat{\mathbf{k}}_\mathbf{F}$ and $+\hat{\mathbf{k}}_\mathbf{F}$ directions, respectively (Fig. 2). To define the positions of the origins O_1 and O_7 in the $\hat{\mathbf{i}}_\mathbf{F}$ and $\hat{\mathbf{j}}_\mathbf{F}$ directions, cylindrical coordinates were used with a radial distance and an angle about $\hat{\mathbf{k}}_\mathbf{F}$. The independent variable β was defined as the angle, projected on the $\hat{\mathbf{i}}_\mathbf{F}\hat{\mathbf{j}}_\mathbf{F}$-plane at full extension, between the $\hat{\mathbf{j}}_\mathbf{F}$ axis and a vector from the origin $\mathrm{F_a}$ to the origin O_1 (Fig. 3); the origin O_7 was positioned with the same $\hat{\mathbf{i}}_\mathbf{F}$ and $\hat{\mathbf{j}}_\mathbf{F}$ coordinates at full extension. The independent variable d was defined to be the distance, projected on the $\hat{\mathbf{i}}_\mathbf{F}\hat{\mathbf{j}}_\mathbf{F}$-plane at full extension, between the origin $\mathrm{F_a}$ and the origins O_1 and O_7 (Fig. 3). The $\hat{\mathbf{i}}_\mathbf{1}$ and $\hat{\mathbf{i}}_\mathbf{7}$ axes were defined to point in the proximal direction at full extension. The orientation of the $\hat{\mathbf{j}}_\mathbf{1}$ axis was defined at full extension by the independent variable γ, defined as the angle, projected on the $\hat{\mathbf{i}}_\mathbf{F}\hat{\mathbf{j}}_\mathbf{F}$-plane at full extension, between the $\hat{\mathbf{j}}_\mathbf{1}$ axis and a vector from the origin $\mathrm{F_a}$ to the origin O_1 (Fig. 3); the $\hat{\mathbf{j}}_\mathbf{7}$ axis was oriented in the same direction as the $\hat{\mathbf{j}}_\mathbf{1}$ axis at full extension. The $\hat{\mathbf{k}}_\mathbf{1}$ and $\hat{\mathbf{k}}_\mathbf{7}$ axes, the revolute axes of links 1 and 7, were defined by the cross product of the $\hat{\mathbf{i}}$ and $\hat{\mathbf{j}}$ axes of links 1 and 7, respectively. The coordinate system of ISL link 1 was fixed to the tibial anatomic coordinate system while the coordinate system of ISL link 7 was fixed to the femoral anatomic coordinate system.

To mathematically describe the relationship between the virtual tibiofemoral joint and the virtual ISL, the ISL transformation matrix $[\mathbf{T}]_\mathbf{ISL}$ was pre- and post-multiplied by two transformation matrixes (Eq. (2))

$$\left[\mathbf{T}_{\mathbf{Fa/Ta}}\right]_2 = \left[\mathbf{T}_{\mathbf{Fa/7}}\right][\mathbf{T}]_\mathbf{ISL}\left[\mathbf{T}_{\mathbf{1/Ta}}\right] \tag{2}$$

where $\left[\mathbf{T}_{\mathbf{Fa/Ta}}\right]_2$ is the transformation matrix from the tibial anatomic coordinate system to the femoral anatomic coordinate system. The transformation matrix $\left[\mathbf{T}_{\mathbf{1/Ta}}\right]$ defined the fixed relationship from the tibial anatomic coordinate system and link 1 of the ISL (Eq. (3)). The transformation matrix $\left[\mathbf{T}_{\mathbf{Fa/7}}\right]$ defined the fixed relationship from link 7 of the ISL to the femoral anatomic coordinate system (Eq. (4)). These transformation matrixes were formulated via consecutive rotation and translation matrix multiplication [38] using five of the independent variables of the ISL (d, β, γ, l, and ϕ) and the radius of the femoral condyles, r_{cond}:

$$\begin{aligned}\left[\mathbf{T}_{\mathbf{1/Ta}}\right] &= \mathrm{Trans}(z, -0.5 \cdot d_{ws} + r_{\mathrm{cond}}) \cdot \mathrm{Rot}(y, -90\,\mathrm{deg}) \\ &\quad \cdot \mathrm{Rot}(x, \beta) \cdot \mathrm{Trans}(y, d) \cdot \mathrm{Rot}(x, \gamma)\end{aligned} \tag{3}$$

$$\begin{aligned}\left[\mathbf{T}_{\mathbf{Fa/7}}\right] &= \mathrm{Rot}(x, -\gamma) \cdot \mathrm{Trans}(y, -d) \cdot \mathrm{Rot}(x, -\beta) \\ &\quad \cdot \mathrm{Rot}(y, 90\,\mathrm{deg}) \cdot \mathrm{Trans}(z, -0.5 \cdot d_{ws})\end{aligned} \tag{4}$$

Because the virtual ISL was rigidly attached to the virtual tibiofemoral joint, the transformation matrixes $\left[\mathbf{T}_{\mathbf{Fa/Ta}}\right]_1$ and $\left[\mathbf{T}_{\mathbf{Fa/Ta}}\right]_2$ were equal (Eq. (5)); thus $[\mathbf{T}]_\mathbf{ISL}$ and therefore the six revolute joint angles of the ISL were a function of the flexion angle and I-E rotation angle of the virtual tibiofemoral joint:

$$\begin{aligned}\left[\mathbf{T}_{\mathbf{Fa/7}}\right][\mathbf{T}]_\mathbf{ISL}\left[\mathbf{T}_{\mathbf{1/Ta}}\right] &= \mathrm{Trans}(z, r_{\mathrm{cond}}) \cdot \mathrm{Trans}(x, 2.5) \cdot \mathrm{Rot}(z, \theta_{I-E}) \\ &\quad \cdot \mathrm{Trans}(x, -2.5) \cdot \mathrm{Rot}(y, -\theta_F)\end{aligned} \tag{5}$$

2.3 Errors in Locating the F-E and LR Axes. Errors in the ISL revolute joint transducers were added to the revolute joint angles throughout simulated tibiofemoral motion. For a given tibiofemoral motion and ISL size and attachment position, the ISL revolute joint angles throughout motion were determined by computing the inverse kinematics [38] of the ISL using MATLAB 7.6.0 (The MathWorks, Natik, MA) and a robotics toolbox [41]. Random errors representing the linearity error (i.e. nonlinearity) in the transducers were added to each set of revolute joint angles; these random errors had a mean of 0 and a standard deviation equal to one half the linearity error of the transducer, or 0.025 deg (DS-25-16, Netzer Precision Motion Sensors Ltd, D.N. Misgav, Israel). The linearity error was approximated by plus and minus two standard deviations to provide a conservative estimate of error in which 95.45% of the random errors are included.

Nonrandom errors representing hysteresis in the transducers were added together with the random nonlinearity errors to each set of revolute joint angles. While mechanical hysteresis of the encoder was stated by the manufacturer to be nonexistent, an induced hysteresis error commonly used in encoders to control signal jitter [42] was simulated to examine possible effects. The maximum hysteresis was simulated as ± 0.5 least significant bits; this corresponded to a maximum hysteresis error of ± 0.044 deg for a 12-bit analog-to-digital converter and a rotational range of 360 deg. The simulated hysteresis error was based on the "ordinary play" model [43], in which the hysteresis error is always the maximum hysteresis error except when the cumulative change in rotation after a change in direction has not yet exceeded twice the maximum hysteresis error. However, due to computational complexity in conjunction with the minimal hysteresis error typical of encoders, the maximum hysteresis error was either added to the nominal revolute joint angles if the difference between the current and previous revolute joint angle was negative, or subtracted if the difference was positive.

The orientation and position errors in locating the F-E and LR axes were determined by calculating new F-E and LR axes; these new axes were determined using an erroneous set of revolute joint angles and the axis-finding method described by Gatti [36]. By subtracting the orientations and positions of the baseline F-E and LR axes from the orientations and positions of the erroneous axes, two orientation errors and two position errors were calculated for each axis. To determine the bias, precision, and RMSE of each of the eight orientation and position errors, new axes were calculated for 200 iterations, each time randomizing the nonlinearity errors (Fig. 4). For "random discrete" motion, the tibiofemoral positions were also randomized in each iteration.

2.4 Optimizing the Independent Variables. The ISL size, attachment position, and pattern of applied motion were optimized by minimizing the RMSE of the eight dependent variables describing the orientations and positions of the F-E and LR axes. First, the ISL size and attachment position were optimized followed by the pattern of applied motion. Because there were eight possible RMSEs to minimize, the largest of the eight RMSEs (i.e. worst-case error) was used to compare each ISL size, attachment

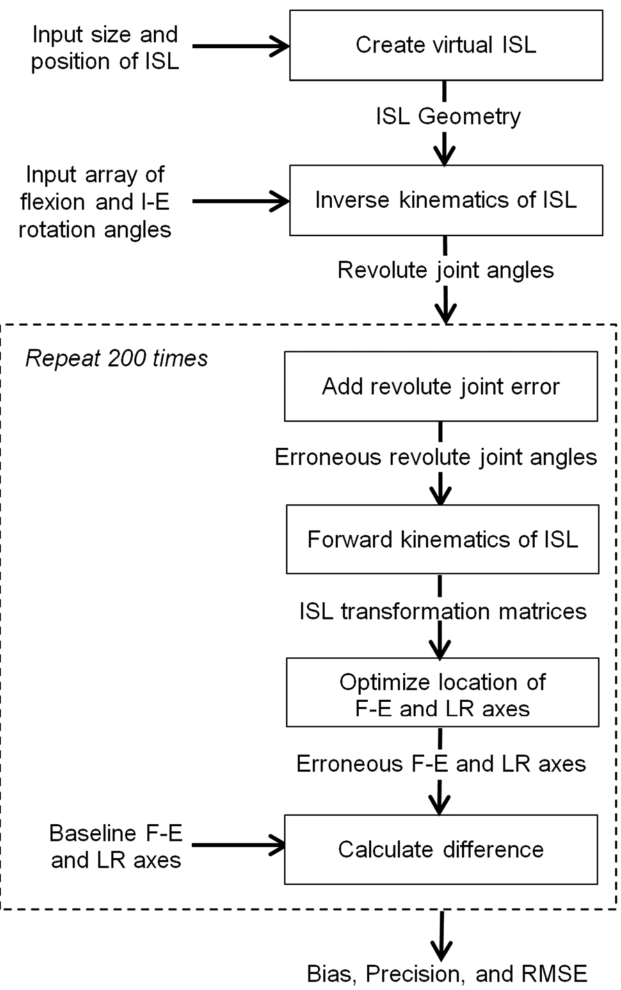

Fig. 4 Flow chart of error calculations

position, and pattern of applied motion. Measurement errors of 1 deg and 1 mm were considered clinically important because surgical errors less than 1 deg and 1 mm are not reliably attained in the operating room during TKA [44–46]. While some dependent variables were measured in millimeters and others in degrees, the magnitudes of the clinically important orientation and position errors were the same (1 deg or 1 mm); thus the applied motion and the ISL size and position that minimized RMSE closest to the clinically important value, in either millimeters or degrees, were chosen.

The ISL size and attachment position were optimized using the "sequential discrete" pattern of applied motion; in this pattern of motion, the resolution between tibiofemoral positions was 5 deg to simulate recording of ISL kinematic data only at discrete flexion and I-E rotation angles. The range of flexion was 120 deg (the approximate limit of passive flexion [47,48]), the I-E rotation range was $\pm$20 deg (the approximate limit of passive I-E rotation [49]), and the number of I-E rotation cycles was seven. This pattern of motion was chosen to optimize the ISL because "sequential continuous" motion was computationally intensive, and "random discrete" motion would not provide consistent applied motions across all ISL configurations. While the envelope of passive I-E rotation changes with flexion angle [49], this was not simulated due to computational complexity and the variability of passive envelopes of motion. The six independent variables describing the size and position of the ISL at full extension were varied given a set of coarse ranges and increments (Table 2) that were chosen to minimize computational complexity yet cover a practical range of possible ISL sizes and attachment positions. The ISL attachment distance d (Fig. 3) was varied from 150 mm

Table 2 The ranges and increments of the independent variables describing the size and attachment position of the ISL

Variable	Range	Increment
d (mm)	150 to 250	50
β (deg)	−90 to +90	45
γ (deg)	−90 to +90	90
l (mm)	200 to 400	100
ϕ (deg)	60 to 150	30
Wrist	Femur or Tibia	–

to 250 mm in increments of 50 mm. The attachment angle of the ISL about the limb, β, was varied from −90 deg to 90 deg in 45 deg increments, simulating a range of attachment positions from anterior to medial to posterior. The attachment orientation of the ISL, γ, was varied from −90 deg to 90 deg in 90 deg increments. The link length, l, (Fig. 2) was varied from 200 mm to 400 mm in 100 mm increments. The ISL "elbow" angle, ϕ, was varied from 60 deg to 150 deg in 30 deg increments. Finally, the ISL "wrist" was either attached to the femur or the tibia. Thus 1080 combinations of the independent variables were defined. The combination of independent variables that minimized the worst-case error in locating the F-E and LR axes defined the optimized ISL.

Prior to error calculation, the ability of a given ISL to reach all positions was verified across a range of motion of 0 deg to 130 deg flexion and $\pm$40 deg I-E rotation, greater than the expected range of motion. Nonconvergence of this verification meant that the ISL either could not reach the entire range of motion or resulted in a singular configuration. The larger range of motion was chosen to ensure that the ISL would reach all necessary positions and orientations on any tibiofemoral joint. In addition, to limit the risk of an ISL colliding with itself, any ISL configuration that reached an "elbow" angle of less than 20 deg throughout the larger range of applied motion was eliminated from the optimization. To check for possible interferences, a solid model of the best-performing ISL was then created in PRO/ENGINEER WILDFIRE 5.0 (PTC, Needham, MA); the model was moved through the full range of motion using the revolute joint angles of the ISL generated in MATLAB and visually checked for interferences between the ISL and a solid model of the tibiofemoral joint.

To determine which of the three patterns of applied motion gave minimal error for the optimized ISL, simulations were performed for each (Table 3). In all three patterns, the range of flexion was 120 deg and the I-E rotation range was $\pm$20 deg. For "sequential discrete" motion, the resolution of applied sequential motion was 5 deg to simulate recording of ISL kinematic data only at discrete flexion and I-E rotation angles. For "sequential continuous" motion, the resolution of applied sequential motion was 0.5 deg to simulate recording of ISL kinematic data throughout continuously applied motion. For "sequential discrete" motion, five different sets of I-E rotation cycles were simulated with 3, 5, 7, 13, and 25 cycles in each set corresponding to 20, 100, 130, 220, and 400 total tibiofemoral positions respectively. For "sequential continuous" motion, the number of I-E rotation cycles was varied from 1 to 24 in increments of 1. For "random discrete" applied motion, five sets of random tibiofemoral positions were simulated. The number of positions in each set of "random discrete" motion was equal to the number of positions in each set of "sequential discrete" motion. The combination of independent variables that minimized the largest position or orientation error in locating the F-E and LR axes defined the best-performing applied motion.

2.5 Sensitivity of Errors to Range of Motion. The axis-finding method using the ISL assumes fixed axes [36]; if either of the axes are not fixed, then it would be necessary to locate the axes using a smaller range of flexion and/or I-E rotation [13]. To

Table 3 The ranges of the independent variables describing the pattern of applied tibiofemoral motion

Type of motion	Variable	Values
"Random discrete"	Number of positions	70, 100, 130, 220, 400
"Sequential discrete"	I-E Rotation resolution (deg)	5
	I-E Rotation cycles	3, 5, 7, 13, 25
"Sequential continuous"	I-E Rotation resolution (deg)	0.5
	I-E Rotation cycles	1 to 24 in increments of 1

investigate how reduced ranges of flexion and I-E rotation affect the orientation and position errors in determining the F-E and LR axes, the independent variables describing maximum flexion and maximum I-E rotation ranges were varied. The maximum flexion range was varied in increasing increments of 10 deg, from 10 deg to 120 deg (i.e. 0–10 deg, 0–20 deg, 0–30 deg, etc.). The maximum I-E rotation range was varied in increments of ± 5 deg, from 0 deg to ± 20 deg. Using the best-performing pattern of applied motion and the best-performing ISL, the bias, precision, and RMSE were calculated for each of the eight dependent variables as a function of the range of flexion and range of I-E rotation.

When applying a smaller flexion arc, the errors may change as a function of the starting flexion angle. To examine this possibility, the flexion arc that maintained all RMSEs below 1 mm and 1 deg was simulated while varying the starting flexion angle in increasing increments of 10 deg until the maximum flexion angle (120 deg) was reached. The I-E rotation range was ± 20 deg.

For the best-performing pattern of applied motion in conjunction with the optimized ISL, the bias, precision, and RMSE were calculated for each of the eight dependent variables. To determine the worst-case errors when using the applied flexion range that maintained all errors below 1 mm and 1°, the maximum bias, precision, and RMS errors at any starting flexion angle were determined.

3 Results

The optimized ISL had the "wrist" attached to the femur, link lengths, $l = 300$ mm, elbow angle, $\phi = 60$ deg, attachment offset, $d = 200$ mm, attachment angle, $\beta = -90$ deg, and attachment orientation, $\gamma = 0$ deg (Fig. 5). Of the 1080 combinations of independent variables, 704 did not converge to a solution, and 309 reached an "elbow angle" of less than 20 deg throughout motion, which left 67 combinations that both converged and maintained an "elbow angle" of at least 20 deg throughout motion. Among the 67 combinations that both converged and maintained an "elbow angle" of at least 20 deg, the maximum RMSE ranged from 0.50 mm to 4.58 mm for the ISLs with the smallest and largest maximum RMSEs, respectively. The ISL that had the smallest maximum RMSE was not chosen because a solid model of this ISL interfered with the virtual knee when simulated in Pro/ENGINEER and instead the next-best ISL was chosen.

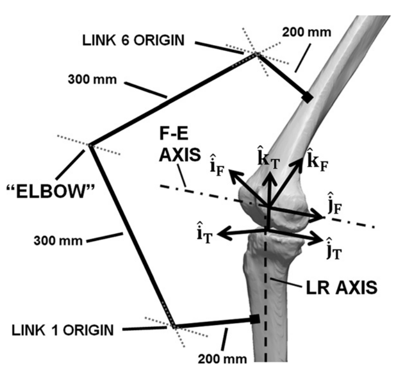

Fig. 5 The optimal ISL had link lengths of 300 mm and was attached to the anterior aspect of the tibiofemoral joint. The axes of the revolute joints of ISL links 1 and 6 were parallel to the F-E axis at full extension, and the "wrist" and "shoulder" were offset 200 mm from the $\hat{k}_F$ axis.

Of the three patterns of applied motion examined, "sequential discrete" was optimal. For all three patterns of applied motion, the M-L RMSE in locating the LR axis was larger than the other errors; thus the M-L error in locating the LR axis was used to compare each of the three applied motions (Fig. 6). Increasing either the number of I-E rotation cycles or random positions decreased the errors for all three cases. While "random discrete" motion minimized the bias error, the precision error in the M-L direction when measuring the LR axis only became lower than 1 mm when the number of tibiofemoral positions was 400 or greater (Fig. 6(*a*)). While "sequential discrete" exhibited higher bias errors in the M-L direction when measuring the LR axis, the precision error was only 0.77 mm at 3 I-E rotation cycles, equivalent to only 70 tibiofemoral positions, and was 0.30 mm at 25 I-E rotation cycles (Fig. 6(*b*)). Thus "sequential" rather than "random" motion improved the precision error by 65% at 70 tibiofemoral positions and by 67% at 400 tibiofemoral positions. At high numbers of I-E rotation cycles, "sequential continuous" motion performed better than "sequential discrete," reducing the precision error by 43% to 0.17 mm; however, the bias error was large and inconsistent, especially at smaller numbers of I-E rotation cycles (Fig. 6(*c*)). Therefore, although "sequential continuous" motion provided the lowest RMSE when the number of I-E rotation cycles was large, "sequential discrete" motion was deemed the optimal motion due to the minimal bias error for any number of I-E rotation cycles.

Using the "sequential discrete" pattern of applied motion in conjunction with the optimized ISL gave negligible errors when locating the F-E and LR axes. For 13 I-E rotation cycles throughout 120 deg flexion and 20 deg I-E rotation, the largest error of the F-E axis was in the A-P direction and the largest error of the LR axis was in the M-L direction (Fig. 7). These errors correspond to overall orientation and position RMSEs of 0.12 deg and 0.39 mm when locating the LR axis, and RMSEs of 0.01 deg and 0.05 mm when locating the F-E axis.

Using the "sequential discrete" pattern of applied motion in conjunction with the optimized ISL, errors when locating the F-E and LR axes increased with decreasing ranges of flexion and I-E rotation. For any range of flexion and I-E rotation with I-E rotation cycles every 5 deg of flexion, the M-L RMSE in locating the LR axis and the P-D RMSE in locating the F-E axes were the two largest errors (Fig. 8). Decreasing the range of I-E rotation minimally increased the P-D RMSE in locating the F-E axis except for when the I-E rotation range was ± 5 deg or ± 0 deg. For I-E rotation ranges of ± 20 deg and ± 15 deg, the P-D RMSE in locating the F-E axis remained below 1 mm for any flexion range between 30 deg and 120 deg; for an I-E rotation range of ± 10 deg, this error remained below 1 mm for any flexion range between 40 deg and 120 deg. Decreasing the range of flexion minimally increased the M-L RMSE in locating the LR axis except for when the I-E rotation range was ± 10 deg or lower. For I-E rotation ranges of ± 20 deg and ± 15 deg, the M-L RMSE in locating the LR axis remained below 1 mm for any flexion range between 20 deg and 120 deg. Thus, the minimum range of motion such that all errors were below 1 mm and 1 deg was 30 deg flexion with ± 15 deg I-E rotation. In addition, the F-E axis could be located without any applied I-E rotation for flexion ranges as low as 50 deg (i.e. 11 data points) while maintaining errors less than 1 mm and 1 deg.

The P-D and A-P RMSEs in locating the F-E axis fluctuated when the starting flexion angle was varied (Fig. 9). The P-D error of the F-E axis approached zero at higher starting flexion angles and reached its maximum when starting from full extension; conversely, the A-P error of the F-E axis increased with starting

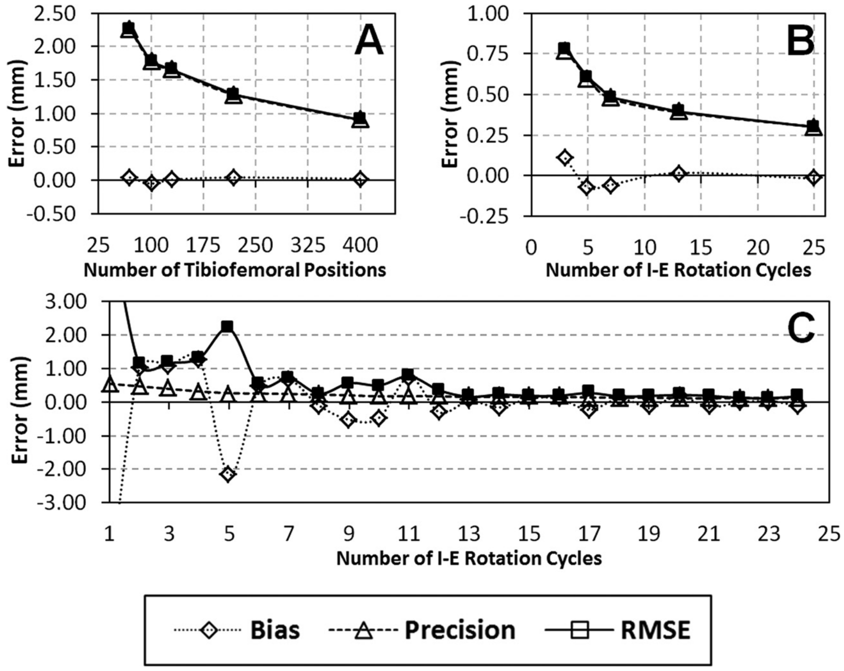

Fig. 6 Bias, precision, and RMSE in locating the LR axis in the M-L direction, for (*a*) "random discrete," (*b*) "sequential discrete," and (*c*) "sequential continuous" patterns of applied motion. "Random discrete" motion had the largest precision error, wile "sequential continuous" motion had the largest bias error.

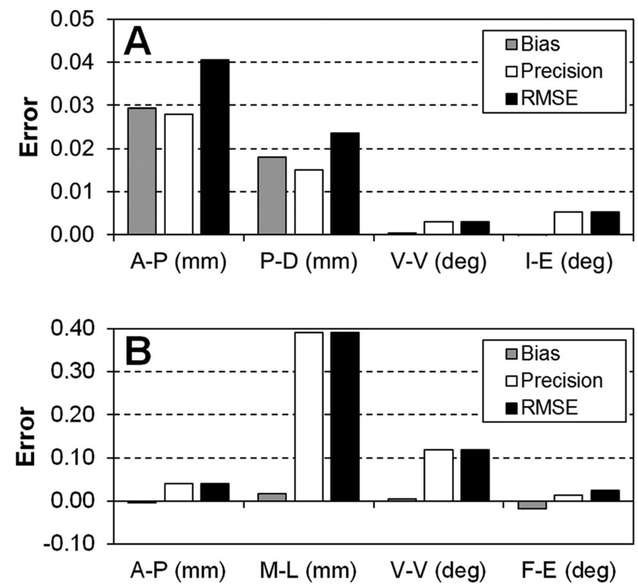

Fig. 7 Bias, precision, and RMSE in locating the (*a*) F-E axis and (*b*) LR Axis, using the optimal ISL and the "sequential discrete" pattern of applied motion for thirteen I-E rotation cycles (±20 deg) across 120 deg flexion. The error in locating the LR axis in the M-L direction was an order of magnitude larger than the errors in locating the F-E axis.

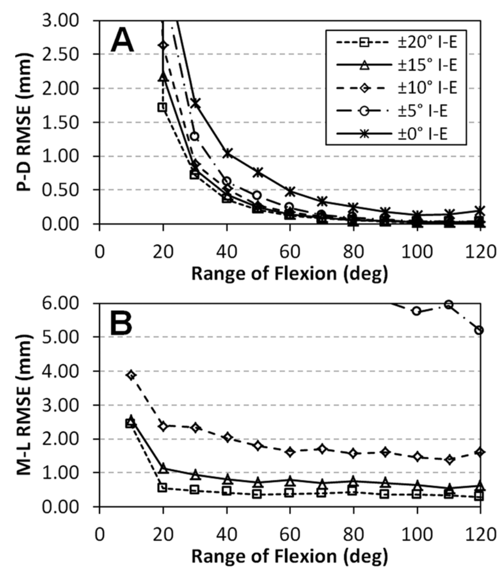

Fig. 8 (*a*) P-D RMSE in locating the F-E axis and (*b*) M-L RMSE in locating the LR axis as a function of range of flexion and range of I-E rotation using "sequential discrete" applied motion. Results for ±5 deg are only partially shown in (*b*) for clarity. The error in locating the F-E axis in the P-D direction was only slightly affected by range of I-E rotation, while the error in locating the LR axis in the M-L direction was only slightly affected by range of flexion.

flexion angle. With a flexion range of 30 deg and an I-E rotation range of ±20 deg, the maximum bias, precision, and RMSE for any of the eight dependent variables at any starting flexion angle was 0.71 mm (Fig. 10).

4 Discussion

Accurately locating the axes of motion is required to accurately characterize kinematics of the tibiofemoral joint. Because errors in locating the F-E and LR axes depend on transducer errors, ISL size and position, and the pattern of applied motion, the first objective was to develop a method to computationally determine the bias, precision, and RMSE in locating these axes due to errors in the revolute joint transducers. Additional objectives were to determine the optimal ISL configuration to minimize these errors, the optimal pattern of the applied motion, and the sensitivity of the errors due to range of flexion and I-E rotation. The method

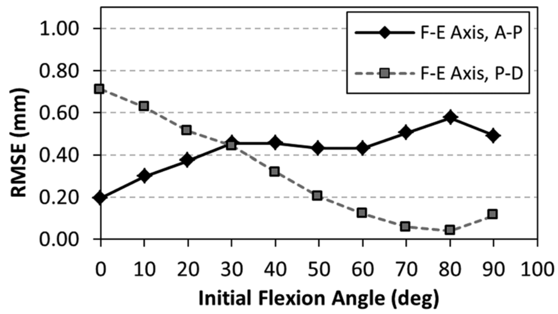

Fig. 9 P-D RMSE and A-P RMSE in locating the F-E axis as a function of initial flexion angle for seven I-E rotation cycles (±20 deg) across 30 deg flexion using the "sequential discrete" pattern of applied motion. While the error in locating the F-E axis was largest in the P-D direction at full extension, the error becomes larger in the A-P direction when starting from 40 deg flexion or greater.

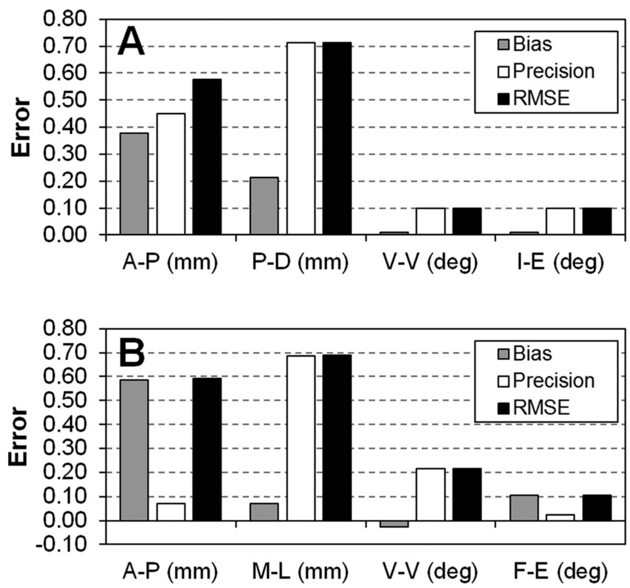

Fig. 10 Maximum bias, precision, and RMSE in locating the (*a*) F-E axis and (*b*) LR axis, using the optimal ISL and the "sequential discrete" pattern of applied motion for seven I-E rotation cycles (±20 deg) across 30 deg flexion at any starting angle

was established and used to determine the optimal ISL configuration. The method showed that "sequential discrete" was the optimal pattern of applied motion because this pattern had lower bias error than the two other patterns of motion for any number of I-E rotation cycles. Finally, to ensure all errors were less than 1 mm or 1 deg, the minimum ranges of "sequential discrete" motion were 30 deg of flexion with ±15 deg of I-E rotation.

The results of the ISL optimization procedure underline the importance of computationally simulating an ISL prior to construction. The inverse kinematics computation for a large proportion the simulated ISL configurations (704/1080) did not converge to a solution, indicating that most ISL sizes and attachment positions are incapable of reaching all tibiofemoral positions throughout the simulated range of motion. Among the remaining 376 ISL configurations that were capable of reaching all required tibiofemoral positions, the "elbow" angle became less than 20 deg throughout the required range of motion for the majority (309/376). Among the 67 successful ISL configurations, the maximum of any of the orientation or position RMSEs for either axis ranged from 0.50 to 4.58 mm; if the ISL was designed without error analysis of a wide range of possible configurations, then errors could be as much as 9 times higher than the minimum. Finally, among those that maintained an "elbow angle" of at least 20 deg and converged to a solution for the entire range of motion, a solid model of the best-performing ISL interfered with a solid model of the tibiofemoral joint during further simulations. As such, omitting any of these simulations would likely result in an ISL that either is incapable of reaching all required positions, collides with itself, has unacceptable error, or interferes with the tibiofemoral joint.

The ISL optimization procedure established design guidelines that were different than the guidelines established by Kirstukas et al. [16]. The previously established guidelines were developed for the measurement of translations and rotations of the tibiofemoral joint rather than the rotational axes. One design guideline was that in general, ISL measurement errors increase with increasing link length [16]; link length was not minimized in our application because the axis-finding method used in this study requires an array of data points across a wide range of flexion and I-E rotation angles. Thus, although minimizing the absolute error at each individual tibiofemoral position was more important when directly measuring motion [16], the range of motion allowed by the ISL was more important when locating rotational axes. Another guideline, that the axis of the first linkage joint should be aligned with the primary rotational axis of the joint [16], was correct for the 14 best-performing linkages because linkages not aligned in this manner were less able to reach all necessary tibiofemoral positions.

To our knowledge, no previous studies that located the F-E and LR axes varied the pattern of applied motion. The Virtual Axis Finder was examined using sequentially applied motion consisting first of incrementally applied I-E rotation followed by flexion with coupled I-E rotation at fixed increments [13]. The error of the axis-finding method used in our study was first examined for one pattern of motion consisting of three I-E rotation cycles applied continuously throughout flexion [36]. When including hysteresis error, this continuous motion would lead to large M-L bias errors when locating the LR axis (Fig. 6). Thus it is important to thoroughly examine each possible pattern of applied motion.

Hysteresis was likely the cause of the increased precision error for "random discrete" motion and the increased bias error for "sequential continuous" motion. For "sequential discrete" motion, the pattern of internal rotation followed by external rotation at fixed flexion angles would remove hysteresis effects caused by I-E rotation. For "random discrete" motion, these rotational errors would not be cancelled by an equal and opposite rotation because all possible combinations of flexion and I-E rotation angles had equal probability. Similarly, in "sequential continuous" motion, the pattern of I-E rotation was different than "sequential discrete" motion in that I-E rotation cycles were applied during constantly applied flexion. The pattern of reciprocating I-E rotation during constant flexion preserves the effects of hysteresis because an equal and opposite rotation does not occur at every flexion angle as in "sequential discrete" motion.

Using the optimal pattern of motion for the full range of motion, the RMSEs were better than previous axis-finding techniques despite the inclusion of linearity and hysteresis errors. Using motion analysis, the Virtual Axis Finder achieved RMSEs of 0.26 deg and 0.28 mm when locating the LR axis and 0.36 deg and 0.25 mm when locating F-E axis after statistically pooling the two orientation errors and two position errors of each axis [13]. To compare the errors of the axis-finding method used in this simulation to those of the Virtual Axis Finder using motion analysis, the same statistically pooled errors were calculated; RMSEs were 0.07 deg and 0.22 mm when locating the LR axis and 0.01 deg and 0.03 mm when locating the F-E axis. All four RMSEs were smaller than those of the Virtual Axis Finder using motion analysis; specifically, the orientation error in locating the LR axis was reduced by 73%, the position error in locating the LR axis was reduced by 21%, the orientation error in locating the F-E axis was reduced by 97%, and the position error in locating the F-E axis was reduced by 88%. Because the Virtual Axis Finder using motion analysis has already been shown to be more accurate than the Mechanical Axis Finder [1,13,14], the axis-finding method described using in conjunction with an ISL [36] is the most accurate axis-finding method available when using the full range of motion.

A smaller range of applied motion may be required if the assumption of fixed axes [1] is not valid, or if range of motion is limited. While studies indicate that the two tibiofemoral axes are fixed [1,3,7], these studies do not apply to reconstructed knees; thus, it is unknown whether this assumption is valid following reconstruction. In addition, because the laxity of the tibiofemoral joint can vary [49], the available range of I-E rotation could be limited. The error in the P-D direction when locating the F-E axis was only slightly affected by the range of I-E rotation except when that range became ± 5 deg or less (Fig. 8). Because knees have an I-E laxity of at least ± 10 deg for the majority of flexion [49], variation of laxity among different limbs should not affect the error in locating the F-E axis. When using an I-E rotation range of at least ± 10 deg, the F-E axis can be located with an error in the P-D direction of less than 1 mm for any flexion range of at least 30 deg, thus a moving F-E axis can be accurately located in 30 deg flexion partitions. Because the Virtual Axis Finder did not use I-E rotation to locate the F-E axis [13], the two methods could not be compared for this case.

An LR axis that moves with flexion can also be located by partitioning the range of flexion. The error in locating the LR axis was affected by the range of I-E rotation more than the error in locating the F-E axis (Fig. 8). Conversely, when the I-E rotation range was at least ± 10 deg, the M-L error when locating the LR axis was relatively unaffected by flexion range except when that range was less than 20 deg. However, to ensure errors of less than 1 mm and 1 deg when locating the LR axis, at least ± 15 deg I-E rotation and 30 deg of flexion is required; thus, an LR axis that moves with flexion could also be accurately located by partitioning flexion into 30 deg increments, provided that the I-E rotation laxity is at least ± 15 deg. While this required I-E rotation range is more than the ± 10 deg of I-E rotation required by the Virtual Axis Finder [13], it is still within the envelope of passive motion [49].

Because the axis-finding method used in this analysis assumes that all motion is about the F-E and LR axes [1,36], additional applied motions such as V-V rotation would reduce accuracy, and thus steps should be taken to prevent the application of these motions. At a flexion angle of 20 deg, the laxity about the LR axis with ± 10 N-m of torsion is approximately 42.3 deg in the unloaded knee [50]. However, ± 1 N-m of V-V torsion causes approximately ± 2 deg of V-V rotation in the unloaded knee at 20 deg of flexion [50]. Thus V-V rotation could be inadvertently applied by I-E torsion that is not precisely about the LR axis. To ensure that V-V rotation is not inadvertently applied, it may be necessary to avoid applying any I-E torsion; with 0 deg of applied I-E rotation 50 deg of flexion is necessary to ensure that both positions and both orientations of the F-E axis have errors of less than 1 mm or 1 deg (Fig. 8). Increasing the range of I-E rotation to ± 5 deg, which would require less than 1 N-m of torsion in the unloaded knee [50], would be unlikely to cause inadvertent V-V rotation and would reduce the required range of flexion to 40 deg while still ensuring that all errors are less than 1 mm and 1 deg. Another possible mitigation is to align the LR axis of the knee with a fixture by removing coupled motions [51]. Alternatively, condylar lift-off could be controlled via an axial load applied along the LR axis that would considerably stiffen the tibiofemoral joint in the V-V degree of freedom [50]. An axial load would also control the inadvertent application of loads in other degrees of freedom such as A-P translation.

There were differences in the way the axis-finding method was implemented in this study when compared with the original description [36]. To locate the LR axis, best-fit plane optimization was implemented using constrained nonlinear minimization via the function fmincon in MATLAB using an active set algorithm rather than the fminsearch function used in the original description [36]. The axes optimized using other minimization algorithms such as fminsearch, fminunc, and simulated annealing were highly dependent upon the initial guess; conversely, the axes optimized using fmincon were independent of the initial guess. To locate the F-E axis, best-fit circles were calculated using Taubin's method [52]; the best-fit circle algorithm used in the original description was not specified [36].

Our method of error analysis achieves several important improvements over previous research. The first is that the method includes both a linearity error and a hysteresis error for each sensor rather than only resolution error [36]. Second, the method presents the resulting errors in terms of anatomic coordinates rather than absolute orientation and position errors [36]. The results of this error analysis indicate that the errors are not equal in each direction and change with flexion (Figs. 7 and 9); furthermore, standard anatomic directions simplify communication between clinicians and biomechanics researchers [53]. Third, the mathematical model presents the errors in terms of bias, precision, and RMSE rather than only RMSE [36]; ignoring the contribution of bias and precision errors to the RMSE would inhibit an accurate comparison of the different patterns of applied motion (Fig. 6).

A similar method could be applied to other joints and/or ISL designs. The method determined the optimal ISL, the optimal applied motion, and the error in locating the F-E and LR axes and was described specifically for the tibiofemoral joint using an equal-link-length "elbow-type" ISL using particular encoders as the revolute transducers. However, this method requires only a virtual model of a joint connected to a virtual ISL and an axis-finding mathematical method specific to the joint. Thus this method could be modified to work with any joint, such as the ankle or shoulder, provided that an axis-finding method is available. In addition, other sensors with other types of errors or other configurations of ISLs could easily be analyzed with this method to optimize an ISL, determine the optimal pattern of applied motion, and determine the expected errors.

There were several limitations in this study. Other errors not included in the method were the error in determining the Denavit–Hartenberg parameters of the ISL [54], compliance of the ISL links [54], play in the revolute joints [54], signal noise, eccentricity of encoder rotation due to assembly error, and signal variation of the rotational transducers due to changes in temperature. Calibration errors and ISL compliance were not simulated due to computation complexity. Play in the revolute joints was not simulated due to computational complexity and because our ISL will be constructed using a previously described bearing assembly with compression screws that eliminates play and separates the revolute joint load from the transducer [55]. Eccentricity was not simulated because the encoders simulated in this study include on-board electronics and calibration procedures to remove the nonlinear effects of mechanical misalignment due to assembly errors. The sensors also convert the analog output signal to a digital serial signal before transmission; thus eliminating signal noise. Finally, sensor variation due to temperature is small and temperature can be easily controlled in a testing environment. If one or more of these additional sources of error were present in an actual ISL used in an experimental setting, then the errors when locating the F-E and LR axes may be different from the computational results. In addition, the error analysis only applies to the optimal ISL configuration; changing parameters such as the attachment distance from the long axes of the femur and tibia or the attachment distance from the F-E axis would change the expected errors.

In summary, we have developed a method for comprehensive analysis of errors when locating the F-E and LR axes using an ISL. This method will aid in the design of ISLs that will be used to locate the F-E and LR axes of the tibiofemoral joint. This analysis is useful when comparing different axis-finding techniques, and has shown that this axis-finding method with the best-performing ISL is comparable or better than the Virtual Axis Finder [13] and thus is the most accurate axis-finding method currently available.

Acknowledgment

We acknowledge the support of the National Science Foundation, Award No. CBET-1067527.

References

[1] Hollister, A. M., Jatana, S., Singh, A. K., Sullivan, W. W., and Lupichuk, A. G., 1993, "The Axes of Rotation of the Knee," Clin. Orthop. Relat. Res., **290**, pp. 259–268.
[2] Eckhoff, D. G., Bach, J. M., Spitzer, V. M., Reinig, K. D., Bagur, M. M., Baldini, T. H., and Flannery, N. M., 2005, "Three-Dimensional Mechanics, Kinematics, and Morphology of the Knee Viewed in Virtual Reality," J. Bone Joint Surg. Am., **87**(Suppl 2), pp. 71–80.
[3] Coughlin, K. M., Incavo, S. J., Churchill, D. L., and Beynnon, B. D., 2003, "Tibial Axis and Patellar Position Relative to the Femoral Epicondylar Axis During Squatting," J. Arthroplasty, **18**(8), pp. 1048–1055.
[4] Most, E., Axe, J., Rubash, H., and Li, G., 2004, "Sensitivity of the Knee Joint Kinematics Calculation to Selection of Flexion Axes," J. Biomech., **37**(11), pp. 1743–1748.
[5] Piazza, S. J., and Cavanagh, P. R., 2000, "Measurement of the Screw-Home Motion of the Knee Is Sensitive to Errors in Axis Alignment," J. Biomech., **33**(8), pp. 1029–1034.
[6] Schache, A. G., Baker, R., and Lamoreux, L. W., 2006, "Defining the Knee Joint Flexion-Extension Axis for Purposes of Quantitative Gait Analysis: An Evaluation of Methods," Gait and Posture, **24**(1), pp. 100–109.
[7] Churchill, D. L., Incavo, S. J., Johnson, C. C., and Beynnon, B. D., 1998, "The Transepicondylar Axis Approximates the Optimal Flexion Axis of the Knee," Clin. Orthop. Relat. Res., **356**, pp. 111–118.
[8] Asano, T., Akagi, M., and Nakamura, T., 2005, "The Functional Flexion-Extension Axis of the Knee Corresponds to the Surgical Epicondylar Axis: *in vivo* Analysis Using a Biplanar Image-Matching Technique," J. Arthroplasty, **20**(8), pp. 1060–1067.
[9] Katz, M. A., Beck, T. D., Silber, J. S., Seldes, R. M., and Lotke, P. A., 2001, "Determining Femoral Rotational Alignment in Total Knee Arthroplasty: Reliability of Techniques," J. Arthroplasty, **16**(3), pp. 301–305.
[10] Incavo, S. J., Coughlin, K. M., Pappas, C., and Beynnon, B. D., 2003, "Anatomic Rotational Relationships of the Proximal Tibia, Distal Femur, and Patella: Implications for Rotational Alignment in Total Knee Arthroplasty," J. Arthroplasty, **18**(5), pp. 643–648.
[11] Eckhoff, D., Hogan, C., Dimatteo, L., Robinson, M., and Bach, J., 2007, "Difference between the Epicondylar and Cylindrical Axis of the Knee," Clin. Orthop. Relat. Res., **461**, pp. 238–244.
[12] Kessler, O., Durselen, L., Banks, S., Mannel, H., and Marin, F., 2007, "Sagittal Curvature of Total Knee Replacements Predicts *in vivo* Kinematics," Clin. Biomech. (Bristol, Avon), **22**(1), pp. 52–58.
[13] Roland, M., Hull, M. L., and Howell, S. M., 2010, "Virtual Axis Finder: A New Method to Determine the Two Kinematic Axes of Rotation for the Tibio-Femoral Joint," J. Biomech. Eng., **132**(1), p. 011009.
[14] Roland, M., Hull, M. L., and Howell, S. M., 2011, "Validation of a New Method for Finding the Rotational Axes of the Knee Using Both Marker-Based Roentgen Stereophotogrammetric Analysis and 3D Video-Based Motion Analysis for Kinematic Measurements," J. Biomech. Eng., **133**(5), p. 051003.
[15] Kinzel, G. L., Hall, A. S., Jr., and Hillberry, B. M., 1972, "Measurement of the Total Motion between Two Body Segments–I. Analytical Development," J. Biomech., **5**(1), pp. 93–105.
[16] Kirstukas, S. J., Lewis, J. L., and Erdman, A. G., 1992, "6r Instrumented Spatial Linkages for Anatomical Joint Motion Measurement—Part I: Design," J Biomech. Eng., **114**(1), pp. 92–100.
[17] Shiavi, R., Limbird, T., Frazer, M., Stivers, K., Strauss, A., and Abramovitz, J., 1987, "Helical Motion Analysis of the Knee–I. Methodology for Studying Kinematics During Locomotion," J. Biomech., **20**(5), pp. 459–469.
[18] Shiavi, R., Limbird, T., Frazer, M., Stivers, K., Strauss, A., and Abramovitz, J., 1987, "Helical Motion Analysis of the Knee–II. Kinematics of Uninjured and Injured Knees During Walking and Pivoting," J. Biomech., **20**(7), pp. 653–665.
[19] Noyes, F. R., Grood, E. S., Cummings, J. F., and Wroble, R. R., 1991, "An Analysis of the Pivot Shift Phenomenon," Am. J. Sports Med., **19**(2), pp. 148–155.
[20] Marans, H. J., Jackson, R. W., Glossop, N. D., and Young, M. C., 1989, "Anterior Cruciate Ligament Insufficiency: A Dynamic Three-Dimensional Motion Analysis," Am. J. Sports Med., **17**(3), pp. 325–332.
[21] Bylski-Austrow, D. I., Grood, E. S., Hefzy, M. S., Holden, J. P., and Butler, D. L., 1990, "Anterior Cruciate Ligament Replacements: A Mechanical Study of Femoral Attachment Location, Flexion Angle at Tensioning, and Initial Tension," J. Orthop. Res., **8**(4), pp. 522–531.
[22] Engebretsen, L., Lew, W. D., Lewis, J. L., and Hunter, R. E., 1990, "The Effect of an Iliotibial Tenodesis on Intraarticular Graft Forces and Knee Joint Motion," Am. J. Sports Med., **18**(2), pp. 169–176.
[23] Gertel, T. H., Lew, W. D., Lewis, J. L., Stewart, N. J., and Hunter, R. E., 1993, "Effect of Anterior Cruciate Ligament Graft Tensioning Direction, Magnitude, and Flexion Angle on Knee Biomechanics," Am. J. Sports Med., **21**(4), pp. 572–581.
[24] Wroble, R. R., Grood, E. S., Cummings, J. S., Henderson, J. M., and Noyes, F. R., 1993, "The Role of the Lateral Extraarticular Restraints in the Anterior Cruciate Ligament-Deficient Knee," Am. J. Sports Med., **21**(2), pp. 257–263.
[25] Wentorf, F. A., Laprade, R. F., Lewis, J. L., and Resig, S., 2002, "The Influence of the Integrity of Posterolateral Structures on Tibiofemoral Orientation When an Anterior Cruciate Ligament Graft Is Tensioned," Am. J. Sports Med., **30**(6), pp. 796–799.
[26] Ishii, Y., Terajima, K., Koga, Y., Takahashi, H. E., Bechtold, J. E., and Gustilo, R. B., 1995, "Comparison of Knee Joint Functional Laxity after Total Knee Replacement with Posterior Cruciate-Retaining and Cruciate-Substituting Prostheses," The Knee, **2**(4), pp. 195–199.
[27] Grood, E. S., Hefzy, M. S., and Lindenfield, T. N., 1989, "Factors Affecting the Region of Most Isometric Femoral Attachments," Am. J. Sports Med., **17**(2), pp. 197–207.
[28] Ishii, Y., Terajima, K., Koga, Y., Takahashi, H., and Bechtold, J., 1996, "Influence of Total Knee Replacement (TKR) Design on Screw-Home Movement: Comparison of Five Designs for Total Knee Replacement Prostheses," J. Orthop. Sci., **1**(5), pp. 313–317.
[29] Ishii, Y., Terajima, K., Terashima, S., Bechtold, J. E., and Laskin, R. S., 1997, "Comparison of Joint Position Sense after Total Knee Arthroplasty," J. Arthroplasty, **12**(5), pp. 541–545.
[30] Sorger, J. I., Federle, D., Kirk, P. G., Grood, E., Cochran, J., and Levy, M., 1997, "The Posterior Cruciate Ligament in Total Knee Arthroplasty," J. Arthroplasty, **12**(8), pp. 869–879.
[31] Ishii, Y., Terajima, K., Koga, Y., Takahashi, H. E., Bechtold, J. E., and Gustilo, R. B., 1998, "Gait Analysis after Total Knee Arthroplasty. Comparison of Posterior Cruciate Retention and Substitution," J. Orthop. Sci., **3**(6), pp. 310–317.
[32] Mannor, D. A., Shearn, J. T., Grood, E. S., Noyes, F. R., and Levy, M. S., 2000, "Two-Bundle Posterior Cruciate Ligament Reconstruction," Am. J. Sports Med., **28**(6), pp. 833–845.
[33] Lewandowski, P. J., Askew, M. J., Lin, D. F., Hurst, F. W., and Melby, A., 1997, "Kinematics of Posterior Cruciate Ligament-Retaining and -Sacrificing Mobile Bearing Total Knee Arthroplasties: An *in vitro* Comparison of the New Jersey LCS Meniscal Bearing and Rotating Platform Prostheses," J. Arthroplasty, **12**(7), pp. 777–784.
[34] Lewis, J. L., Lew, W. D., and Schmidt, J., 1988, "Description and Error Evaluation of an *in vitro* Knee Joint Testing System," J. Biomech. Eng., **110**(3), pp. 238–248.
[35] Kinzel, G. L., Hillberry, B. M., Hall, A. S., Jr., Van Sickle, D. C., and Harvey, W. M., 1972, "Measurement of the Total Motion between Two Body Segments – II Description of Application," J. Biomech., **5**(3), pp. 283–293.
[36] Gatti, G., 2012, "On the Estimate of the Two Dominant Axes of the Knee Using an Instrumented Spatial Linkage," J. Appl. Biomech., **28**(2), pp. 200–209.
[37] Howell, S. M., Howell, S. J., and Hull, M. L., 2010, "Assessment of the Radii of the Medial and Lateral Femoral Condyles in Varus and Valgus Knees With Osteoarthritis," J. Bone Joint Surg. Am., **92A**(1), pp. 98–104.
[38] Paul, R. P., 1981, *Robot Manipulators: Mathematics, Programming, and Control*, MIT Press, Cambridge, MA.
[39] Uicker, J., Denavit, J., and Hartenberg, R. S., 1964, "An Iterative Method for the Displacement Analysis of Spatial Mechanisms," J. Appl. Mech., **31**, pp. 309–314.
[40] Paden, B., and Sastry, S., 1988, "Optimal Kinematic Design of 6r Manipulators," Int. J. Robot Res., **7**(2), pp. 43–61.
[41] Corke, P. I., 1996, "A Robotics Toolbox for Matlab," IEEE Robot Autom. Mag., **3**(1), pp. 24–32.
[42] Mayer, J. R. R., 1994, "High-Resolution of Rotary Encoder Analog Quadrature Signals," IEEE Trans. Inst. Meas., **43**(3), pp. 494–498.
[43] Krasnosel'skiĭ, M. A., and Pokrovskiĭ, A. V., 1989, *Systems with Hysteresis, Universitext*, Springer-Verlag, Berlin.
[44] Nabeyama, R., Matsuda, S., Miura, H., Mawatari, T., Kawano, T., and Iwamoto, Y., 2004, "The Accuracy of Image-Guided Knee Replacement Based on Computed Tomography," J. Bone Joint Surg. Br., **86**(3), pp. 366–371.
[45] Mizu-Uchi, H., Matsuda, S., Miura, H., Okazaki, K., Akasaki, Y., and Iwamoto, Y., 2008, "The Evaluation of Post-Operative Alignment in Total Knee Replacement Using a CT-Based Navigation System," J. Bone Joint Surg. Br., **90**(8), pp. 1025–1031.
[46] Mizu-Uchi, H., Matsuda, S., Miura, H., Higaki, H., Okazaki, K., and Iwamoto, Y., 2009, "Three-Dimensional Analysis of Computed Tomography-Based Navigation System for Total Knee Arthroplasty: The Accuracy of Computed Tomography-Based Navigation System," J. Arthroplasty, **24**(7), pp. 1103–1110.
[47] Freeman, M. A., and Pinskerova, V., 2005, "The Movement of the Normal Tibio-Femoral Joint," J. Biomech., **38**(2), pp. 197–208.
[48] Freeman, M. A., and Pinskerova, V., 2003, "The Movement of the Knee Studied by Magnetic Resonance Imaging," Clin. Orthop. Relat. Res., **410**, pp. 35–43.
[49] Blankevoort, L., Huiskes, R., and De Lange, A., 1988, "The Envelope of Passive Knee Joint Motion," J. Biomech., **21**(9), pp. 705–720.

[50] Markolf, K. L., Bargar, W. L., Shoemaker, S. C., and Amstutz, H. C., 1981, "The Role of Joint Load in Knee Stability," J. Bone Joint Surg. Am., **63**(4), pp. 570–585.
[51] Bach, J. M., and Hull, M. L., 1995, "A New Load Application System for *in vitro* Study of Ligamentous Injuries to the Human Knee Joint," J. Biomech. Eng., **117**(4), pp. 373–382.
[52] Taubin, G., 1991, "Estimation of Planar Curves, Surfaces, and Nonplanar Space-Curves Defined by Implicit Equations With Applications to Edge and Range Image Segmentation," IEEE Trans. Pattern Anal. Mach. Intell., **13**(11), pp. 1115–1138.
[53] Grood, E. S., and Suntay, W. J., 1983, "A Joint Coordinate System for the Clinical Description of Three-Dimensional Motions: Application to the Knee," J. Biomech. Eng., **105**(2), pp. 136–144.
[54] Suntay, W. J., Grood, E. S., Hefzy, M. S., Butler, D. L., and Noyes, F. R., 1983, "Error Analysis of a System for Measuring Three-Dimensional Joint Motion," J. Biomech. Eng., **105**(2), pp. 127–135.
[55] Nordquist, J., and Hull, M. L., 2007, "Design and Demonstration of a New Instrumented Spatial Linkage for Use in a Dynamic Environment: Application to Measurement of Ankle Rotations During Snowboarding," J. Biomech. Eng., **129**(2), pp. 231–239.